Frequency offset Raman spectroscopy (FORS) for depth probing of diffusive media

SANATHANA KONUGOLU VENKATA SEKAR,[1,*] SARA MOSCA,[1] ANDREA FARINA,[2] FABRIZIO MARTELLI,[3] PAOLA TARONI,[1,2] GIANLUCA VALENTINI,[1,2] RINALDO CUBEDDU,[1] AND ANTONIO PIFFERI[1,2]

[1]*Dipartimento di Fisica, Politecnico di Milano, Milano, Italy, Piazza Leonardo da Vinci 32, 20133, Milano, Italy*
[2]*Istituto di Fotonica e Nanotecnologie, Consiglio Nazionale delle Ricerche, Piazza Leonardo da Vinci 32, 20133 Milano, Italy*
[3]*Università degli Studi di Firenze, Dipartimento di Fisica e Astronomia, Via G. Sansone 1, 50019 Sesto Fiorentino, Firenze, Italy.*
**sanathana.konugolu@polimi.it*

Abstract: We present a new technique, frequency offset Raman spectroscopy (FORS), to probe Raman spectra of diffusive media in depth. The proposed methodology obtains depth sensitivity exploiting changes in optical properties (absorption and scattering) with excitation wavelengths. The approach was demonstrated experimentally on a two-layer tissue phantom and compared with the already consolidated spatially offset Raman spectroscopy (SORS) technique. FORS attains a similar enhancement of signal from deep layers as SORS, namely 2.81 against 2.62, while the combined hybrid FORS-SORS approach leads to a markedly higher 6.0 enhancement. Differences and analogies between FORS and SORS are discussed, suggesting FORS as an additional or complementary approach for probing heterogeneous media such as biological tissues in depth.

OCIS codes: (170.5660) Raman spectroscopy; (170.7050) Turbid media; (290.0290) Scattering; (290.5860) Scattering, Raman; (300.6500) Spectroscopy, time-resolved.

References and links

1. R. Petry, M. Schmitt, and J. Popp, "Raman spectroscopy-a prospective tool in the life sciences," ChemPhysChem **4**(1), 14–30 (2003).
2. P. Matousek and N. Stone, "Recent advances in the development of Raman spectroscopy for deep non-invasive medical diagnosis," J. Biophotonics **6**(1), 7–19 (2013).
3. Z. Movasaghi, S. Rehman, and I. U. Rehman, "Raman spectroscopy of biological tissues," Appl. Spectrosc. Rev. **42**(5), 493–541 (2007).
4. A. Rae, R. Stosch, P. Klapetek, A. R. Hight Walker, and D. Roy, "State of the art Raman techniques for biological applications," Methods **68**(2), 338–347 (2014).
5. C. R. Flach and D. J. Moore, "Infrared and Raman imaging spectroscopy of ex vivo skin," Int. J. Cosmet. Sci. **35**(2), 125–135 (2013).
6. P. J. Caspers, G. W. Lucassen, and G. J. Puppels, "Combined in vivo confocal Raman spectroscopy and confocal microscopy of human skin," Biophys. J. **85**(1), 572–580 (2003).
7. M. Mélot, P. D. A. Pudney, A. M. Williamson, P. J. Caspers, A. Van Der Pol, and G. J. Puppels, "Studying the effectiveness of penetration enhancers to deliver retinol through the stratum cornum by in vivo confocal Raman spectroscopy," J. Control. Release **138**(1), 32–39 (2009).
8. P. Matousek, I. P. Clark, E. R. C. Draper, M. D. Morris, A. E. Goodship, N. Everall, M. Towrie, W. F. Finney, and A. W. Parker, "Subsurface probing in diffusely scattering media using spatially offset Raman spectroscopy," Appl. Spectrosc. **59**(4), 393–400 (2005).
9. M. D. Keller, S. K. Majumder, and A. Mahadevan-Jansen, "Spatially offset Raman spectroscopy of layered soft tissues," Opt. Lett. **34**(7), 926–928 (2009).
10. P. Matousek, C. Conti, M. Realini, and C. Colombo, "Micro-scale spatially offset Raman spectroscopy for non-invasive subsurface analysis of turbid materials," Analyst (Lond.) **141**(3), 731–739 (2016).
11. B. Gardner, P. Matousek, and N. Stone, "Temperature spatially offset Raman spectroscopy (T-SORS): subsurface chemically specific measurement of temperature in turbid media using anti-stokes spatially offset Raman spectroscopy," Anal. Chem. **88**(1), 832–837 (2016).
12. K. M. Khan, S. K. Majumder, and P. K. Gupta, "Cone-shell Raman spectroscopy (CSRS) for depth-sensitive measurements in layered tissue," J. Biophotonics **8**(11-12), 889–896 (2015).

13. K. M. Khan, N. Ghosh, and S. K. Majumder, "Off-confocal Raman spectroscopy (OCRS) for subsurface measurements in layered turbid samples," J. Opt. **18**(9), 095301 (2016).
14. K. Buckley and P. Matousek, "Recent advances in the application of transmission Raman spectroscopy to pharmaceutical analysis," J. Pharm. Biomed. Anal. **55**(4), 645–652 (2011).
15. I. E. Iping Petterson, P. Dvořák, J. B. Buijs, C. Gooijer, and F. Ariese, "Time-resolved spatially offset Raman spectroscopy for depth analysis of diffusely scattering layers," Analyst (Lond.) **135**(12), 3255–3259 (2010).
16. M. D. Morris and G. S. Mandair, "Raman assessment of bone quality," Clin. Orthop. Relat. Res. **469**(8), 2160–2169 (2011).
17. P. I. Okagbare, D. Begun, M. Tecklenburg, A. Awonusi, S. A. Goldstein, and M. D. Morris, "Noninvasive Raman spectroscopy of rat tibiae: approach to in vivo assessment of bone quality," J. Biomed. Opt. **17**(9), 090502 (2012).
18. P. Matousek and N. Stone, "Prospects for the diagnosis of breast cancer by noninvasive probing of calcifications using transmission Raman spectroscopy," J. Biomed. Opt. **12**(2), 024008 (2007).
19. B. Brozek-Pluska, J. Musial, R. Kordek, E. Bailo, T. Dieing, and H. Abramczyk, "Raman spectroscopy and imaging: applications in human breast cancer diagnosis," Analyst (Lond.) **137**(16), 3773–3780 (2012).
20. K. Buckley, J. G. Kerns, P. D. Gikas, H. L. Birch, J. Vinton, R. Keen, A. W. Parker, P. Matousek, and A. E. Goodship, "Measurement of abnormal bone composition in vivo using noninvasive Raman spectroscopy," IBMS boneKEy **11**(602), 1–3 (2014).
21. C. Eliasson and P. Matousek, "Noninvasive authentication of pharmaceutical products through packaging using spatially offset Raman spectroscopy," Anal. Chem. **79**(4), 1696–1701 (2007).
22. K. Buckley and P. Matousek, "Non-invasive detection of concealed liquid and powder explosives using spatially offset Raman spectroscopy," in Infrared and Raman Spectroscopy in Forensic Science, J. M. Chalmers, H. G. M. Edwards, and M. D. Hargreaves, eds (Wiley, 2012).
23. J. Qin, K. Chao, and M. S. Kim, "Nondestructive evaluation of internal maturity of tomatoes using spatially offset Raman spectroscopy," Postharvest Biol. Technol. **71**, 21–31 (2012).
24. C. Conti, C. Colombo, M. Realini, and P. Matousek, "Subsurface analysis of painted sculptures and plasters using micrometre-scale spatially offset Raman spectroscopy (micro-SORS)," J. Raman Spectrosc. **46**(5), 476–482 (2015).
25. S. Del Bianco, F. Martelli, and G. Zaccanti, "Penetration depth of light re-emitted by a diffusive medium: theoretical and experimental investigation," Phys. Med. Biol. **47**(23), 4131–4144 (2002).
26. F. Martelli, T. Binzoni, A. Pifferi, L. Spinelli, A. Farina, and A. Torricelli, "There's plenty of light at the bottom: statistics of photon penetration depth in random media," Sci. Rep. **6**, 27057 (2016).
27. A. P. Shreve, N. J. Cherepy, and R. A. Mathies, "Effective rejection of fluorescence interference in Raman spectroscopy using a shifted excitation difference technique," Appl. Spectrosc. **46**(4), 707–711 (1992).
28. M. Elias, "Relationship between the size distribution of mineral pigments and color saturation," Appl. Opt. **50**(16), 2464–2473 (2011).
29. G. Latour, M. Elias, and J. M. Frigerio, "Determination of the absorption and scattering coefficients of pigments: application to the identification of the components of pigment mixtures," Appl. Spectrosc. **63**(6), 604–610 (2009).
30. P. Matousek, M. D. Morris, N. Everall, I. P. Clark, M. Towrie, E. Draper, A. Goodship, and A. W. Parker, "Numerical simulations of subsurface probing in diffusely scattering media using spatially offset Raman spectroscopy," Appl. Spectrosc. **59**(12), 1485–1492 (2005).
31. F. Martelli, T. Binzoni, S. K. Sekar, A. Farina, S. Cavalieri, and A. Pifferi, "Time-domain Raman analytical forward solvers," Opt. Express **24**(18), 20382–20399 (2016).
32. B. H. Hokr and V. V. Yakovlev, "Raman signal enhancement via elastic light scattering," Opt. Express **21**(10), 11757–11762 (2013).
33. P. Matousek, "Inverse spatially offset Raman spectroscopy for deep noninvasive probing of turbid media," Appl. Spectrosc. **60**(11), 1341–1347 (2006).
34. I. E. Iping Petterson, F. W. L. Esmonde-White, W. de Wilde, M. D. Morris, and F. Ariese, "Tissue phantoms to compare spatial and temporal offset modes of deep Raman spectroscopy," Analyst (Lond.) **140**(7), 2504–2512 (2015).
35. P. Taroni, A. Bassi, D. Comelli, A. Farina, R. Cubeddu, and A. Pifferi, "Diffuse optical spectroscopy of breast tissue extended to 1100 nm," J. Biomed. Opt. **14**(5), 054030 (2009).
36. A. Pifferi, A. Torricelli, P. Taroni, A. Bassi, E. Chikoidze, E. Giambattistelli, and R. Cubeddu, "Optical biopsy of bone tissue: a step toward the diagnosis of bone pathologies," J. Biomed. Opt. **9**(3), 474–480 (2004).
37. S. Konugolu Venkata Sekar, A. Dalla Mora, I. Bargigia, E. Martinenghi, C. Lindner, P. Farzam, M. Pagliazzi, T. Durduran, P. Taroni, A. Pifferi, and A. Farina, "Broadband (600-1350 nm) Time-Resolved Diffuse Optical Spectrometer for Clinical Use," IEEE J. Sel. Top. Quantum Electron. **22**(3), 7349112 (2016).
38. S. Konugolu Venkata Sekar, A. Farina, E. Martinenghi, A. Dalla Mora, P. Taroni, A. Pifferi, T. Durduran, M. Pagliazzi, C. Lindner, P. Farzam, M. Mora, M. Squarcia, and U. Ispizua, "Broadband time-resolved diffuse optical spectrometer for clinical diagnostics: characterization and in-vivo measurements in the 600-1350 nm spectral range," Eur. Conf. Biomed. Opt. **9538**, 95380R (2015).
39. D. Contini, F. Martelli, and G. Zaccanti, "Photon migration through a turbid slab described by a model based on diffusion approximation. I. Comparison with Monte Carlo results," Appl. Opt. **36**(19), 4587–4599 (1997).

40. R. C. Haskell, L. O. Svaasand, T. T. Tsay, T. C. Feng, M. S. McAdams, and B. J. Tromberg, "Boundary conditions for the diffusion equation in radiative transfer," J. Opt. Soc. Am. A **11**(10), 2727–2741 (1994).

1. Introduction

Excellent chemical specificity and sensitivity to structural changes of molecules have made Raman spectroscopy a promising tool for probing biological samples [1–4]. Yet, most often Raman spectroscopy was limited to *ex vivo* sample analysis [5] or *in vivo* analysis of the superficial layer with depths around few hundred microns [6,7]. The high scattering nature of biological tissues poses problems for deep tissue profiling. However, the recent invention of Spatial Offset Raman Spectroscopy (SORS) [8,9] has led to the development of sister techniques (μ-SORS [10], T-SORS [11], CSRS [12], OCRS [13]), and to the renaissance of Transmission Raman [14] and of Time Resolved Raman spectroscopy (TRR) [15]. SORS has brought major advancement in Raman spectroscopy of deep tissue in biological media. In recent years, increased attention has been dedicated, as few examples, to the study of bone mineral assessment [16,17], breast cancer detection [18,19], characterisation of pathologic bone [20], pharmaceutical assessment of tablets [21], and also, in other fields, detection of explosives [22], food monitoring [23], non-destructive analysis of works of art [24].

SORS works on the principle of getting deeper information (bottom layer) on a medium by increasing the source-detector separation (d) in order to exploit a well-known spatial characteristic of light propagation in diffusing media. Though SORS has been a pioneer technique for deep material analysis, it suffers from low signal to noise ratio (SNR) at large source-detector separation, and reduction in spatial resolution due to changing probed volume upon increasing d. Time-Resolved Raman spectroscopy employs the temporal characteristics of light propagation in diffusive media to extract the Raman signal of deeper layers. Indeed, late photons in the temporal profile carry depth information [25,26]. In brief, SORS and TRR utilise, respectively, spatial and temporal nature of photon propagation in diffuse media to collect Raman signal from a specific depth in highly scattering media.

We propose an alternative approach, named Frequency Offset Raman Spectroscopy (FORS), which achieves different depth probing exploiting the spectral dependence of the optical properties (absorption and reduced scattering coefficients, μ_a and μ'_s respectively) of the diffusive medium to be characterized. Though the idea of frequency shift by a small fraction was proposed in the past for fluorescence background correction [27], it has never been used for depth probing.

Aim of our work is to demonstrate FORS as a novel technique to retrieve deep layer information. A dedicated tissue mimicking phantom with optical properties relevant to biological media was exploited to perform a comparison between SORS and FORS, and highlight the complementary nature and general relation between them. In the end, a novel FORS-SORS technique is proposed to harvest the benefits of both techniques to enhance Raman detection from deeper layers.

2. Frequency offset Raman spectroscopy (FORS)

The optical properties are intrinsic nature to a given specific medium, and vary with the frequency (wavelength) of light. The mean depth explored by the photons collected at a distance d from the injection point depends on the value assumed by the optical properties of the medium [26]. Hence, depth probing can be achieved by exploiting the different values of the optical properties of the medium at different frequencies. Thus, by performing Raman spectroscopy at different excitation frequencies it is possible to selectively probe different parts of medium, provided that different optical properties versus frequency are observed. This idea is the basic principle of FORS.

In a diffusive medium or in general in a scattering medium, high absorption values prevent the photons propagation in the deep part of the medium. Hence, in the case of high absorption the FORS signal is dominated by the top layer, whereas under low absorption

conditions the contribution from the bottom layer increases. This fact means that a maximum absorption contrast gives rise to a maximum Raman signal contrast between top and bottom layer. Similarly, high scattering increases the Raman signal of the top layer, and prevents the photon migration in the deeper part of the medium, which decreases significantly the contribution of the bottom layer. This fact also means that the bottom layer contribution can be increased by decreasing the scattering of the medium. Thus, scattering contrast versus frequency gives rise to Raman signal contrast between top and bottom layer. In SORS, maximum contrast of the signal between top and bottom layer is achieved by maximum contrast in the signal at two values of the source-detector separation *d*. Differently, in FORS maximum contrast can be achieved by maximum absorption and scattering contrast, which in turn can be achieved by changing Raman excitation frequency. The spatial resolution in FORS can be particularly high, as it is performed at a single source-detector separation, whilst with SORS the resolution is hampered by the fact that the measurements are performed at different source-detector separations, and thus probe distinct volumes. Table 1 gives a general qualitative overview and a brief comparison between SORS and FORS techniques. For getting a more quantitative comparison between SORS and FORS a modelling of the two techniques is required. Martelli et al. presented a detailed description of the photon penetration depths inside a slab [26]. The approach is strictly applicable only in the diffusive regime and for elastic scattering. Still, this approach could also be re-adapted with good reliability to estimate the photon penetration depth in Raman scattering measurements.

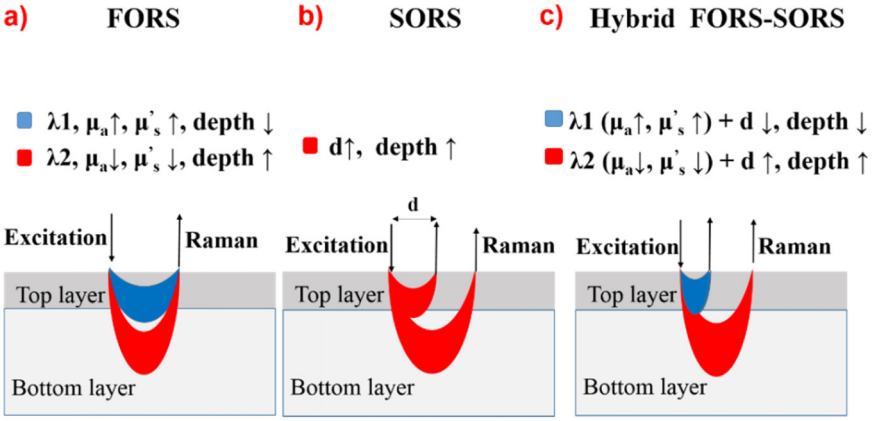

Fig. 1. The principles of FORS (a), SORS (b) and hybrid FORS-SORS (c) are shown.

Table 1. Comparison between SORS and FORS in term of their main features.

	SORS	FORS
Contrast	Achieved by changing source-detector separation (*d*)	Achieved by changing excitation frequency (changing optical properties μ_a and μ'_s)
Signal to noise ratio (SNR)	Low SNR at large source-detector separation	High SNR, as the source-detector separation can be kept minimum
Spatial resolution	Low spatial resolution due to operation at various *d* values	High spatial resolution, as *d* can be kept constant and minimum
Enhancement of deep layer information	Limited by *d* (low SNR)	Limited by optical properties contrast, higher contrast leads to higher enhancement

The idea of FORS is relevant to biological media. In general, scattering decreases by increasing wavelength, while the absorption depends on the dominant tissue constituents of

the tissue under study and on the wavelength range considered. Most of the tissue constituents (*e.g.*, oxy-hemoglobin, deoxy-hemoglobin, lipid, water, collagen) have an intrinsic absorption coefficient that varies significantly versus wavelength, which is a necessary condition for FORS. Apart from applications involving biological media, the proposed technique can be relevant for any medium where a contrast in optical properties is seen by changing the excitation wavelength. Specific cases of pharmaceutical tablets assessment, art work conservation, fruits and vegetables quality control are few potential areas. For example, when dealing with the investigation of painted artworks both the pigment nature and its size inside the binder matrix can provide absorption and scattering changes [28,29].

In general, even when dealing with SORS, the medium optical properties have a great effect on the depth reached by probing photons. A proper and careful evaluation of the optical properties of the medium could provide valuable information for improving sensitivity and quantitation of the technique used. The study of photon propagation in diffusive media (Diffuse Optics) has vastly expanded over the last decades with a wide arsenal of models, methods, techniques, devices. Translation of this deep know-how into the field of Diffuse Raman is still in its infancy [30–32], and great advancements are expected by this cross-fertilization.

Experimentally, FORS measurements can be realised by performing Raman measurements at multiple excitation wavelengths, where the medium under study has different optical properties (μ_a and μ'_s). This principle is depicted in Fig. 1(a): at wavelength $\lambda 1$, the medium has higher μ_a and μ'_s, preventing photons from reaching deeper layers. Accordingly, the measurement is dominated by Raman signal from the top layer. However, at wavelength $\lambda 2$, the medium possesses lower μ_a and μ'_s values, so that photons propagate deeper, which increases the contribution of the bottom layer to the acquired signal. Intuitively, it can be seen from Fig. 1(a): higher the contrast of the optical properties at $\lambda 1$ and $\lambda 2$, lower will be the contamination of signal between the two layers, and eventually a higher contrast will be achieved in FORS measurements.

3. Experimental

3.1 Setup

Figure 2 shows the schematic of the experimental setup. Our Raman probe works similar to the inverse SORS configuration [33], with ring illumination source and point collection, and is connected to the excitation laser and to the spectrometer through fiber optics. It was specifically designed to perform SORS and FORS measurements in a non-contact geometry, using multi-wavelength excitation (700 nm, 745 nm, 780 nm, 808 nm).

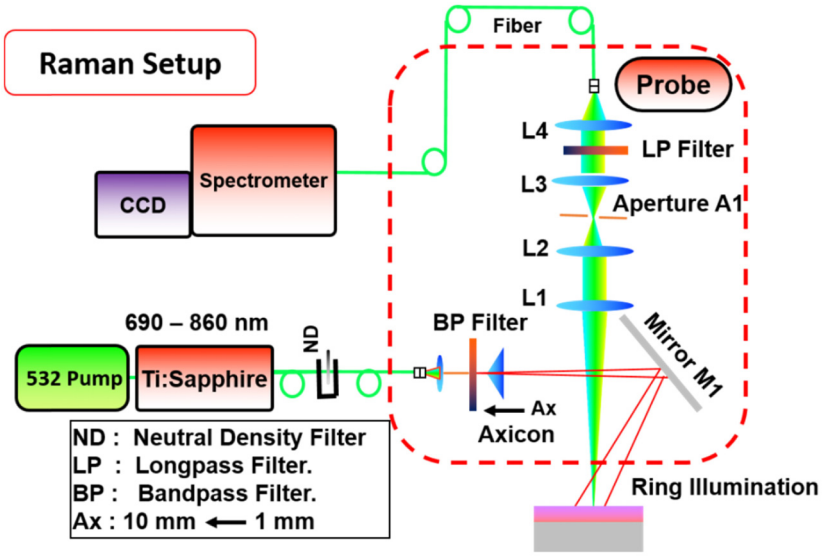

Fig. 2. Experimental setup for SORS and FORS measurements. The Raman probe is demarcated with a red dashed line.

A Ti:Sapphire laser pumped by 532 nm light from a frequency doubled Nd:YAG laser provides a tunable laser source in the 690-860 nm range. A 100 µm optical fiber couples the light from the laser to a collimator in the Raman probe, built using Thorlabs 30 mm diameter cage system. Depending on the excitation wavelength, a suitable 10 nm bandwidth bandpass filter (700 nm,750 nm, 780 nm, 810 nm) is used to clean the laser beam. An Axicon lens (UV fused silica axicon element with a cone angle $\alpha = 5°$) is then exploited to create ring illumination. Mirror M1 (silver mirror) reflects the ring source onto the sample. The radius of the ring illumination can be varied from 1 mm to 10 mm by moving the Axicon on its railing away from mirror M1. Cross positioning of mirror M1 and the corresponding incidence direction, slightly tilted with respect to normal incidence, distort only negligibly the shape of the ring. The source-detector separation d is calculated between the center of point collection and the inner radius of ring illumination. The collection system involves a set of four optical lenses (diameter 25 mm) with effective f-number f/2. L2 and L3 along with a narrow aperture (A1) act as a Fourier optical low pass filter system, which enhances point collection and prevents stray light from entering the detection system. A suitable long pass filter (715 nm, 750 nm, 785 nm, 808 nm) is placed between lenses L3 and L4 to remove the excitation photons effectively. L4 couples the Raman signal into a 1 mm optical fiber, which transfers the light to a spectrometer (Acton SpectraPro2150, Princeton Instruments, f/4 system, grating 1200 grooves/mm) through a 200 µm slit. A cooled CCD camera (iDUS DV401A, Andor Technology Ltd., 1024 × 255, pixel size 26 × 26 μm^2) is used to record Raman spectra. The CCD is vertically binned to increase signal intensity, while maintaining spectral resolution.

3.2 Phantom preparation and characterization

The tissue mimicking phantom to demonstrate FORS consists of two layers. The top layer was made of a silicone elastomer (polydimethylsiloxane PDMS, Sylgard) and has cylindrical shape (radius = 30 mm, thickness = 10 mm). The bottom layer is a rectangular marble slab (calcite $CaCO_3$, 40 × 30 mm^2, thickness = 17 mm).

Silicone elastomer has been used commonly in diffuse optics and Raman spectroscopy to mimic tissue optical properties [34]. The scattering properties of PDMS were tailored to be μ'_s = 10 cm^{-1} (typical near-infrared scattering of biological tissue) at 700 nm, which was achieved by mixing a mild quantity of TiO_2 powder to the PDMS recipe. Printer ink (Cyan)

of calculated quantity was added to the recipe to produce absorption μ_a = 0.18 cm^{-1} at 700 nm. Importantly, cyan ink shows sharp absorption changes in the 700–800 nm range, which is a key feature for FORS measurements.

The optical properties (μ_a and μ'_s) of the PDMS layer were characterised using time domain diffuse optical spectroscopy, which is a typical methodology applied for characterising *in vivo* biological tissues, and more generally highly diffusive media in the near-infrared range [35,36]. Broadband time-resolved measurements were performed using a diffuse optical spectrometer over the 600-880 nm range. A detailed description of the instrumentation is presented elsewhere [37,38]. The temporal curves measured at each wavelength were fitted to a solution of the Diffusion equation [39] with extrapolated boundary condition [40] to extract μ_a, and μ'_s of PDMS. The extracted spectra are presented and discussed in the following sections.

3.3 Experimental protocol and data analysis

The measurement protocol consists of two parts. At first conventional SORS measurements were performed at 780 nm with multiple source-detector separations (d = 1 mm, 4.5 mm, 10 mm). These measurements validated our system with traditional SORS, and acted as a standard to compare with FORS technique. Then, FORS measurements were performed at multiple excitations (700 nm, 745 nm, 780 nm, 808 nm) with constant source-detector separation (d = 4.5 mm). A schematic of the measurement geometry is shown in Fig. 3. Furthermore, SORS and FORS measurements at all possible combinations (SORS at all excitations and FORS at all source-detector separations) were performed. This provided an overall picture of SORS and FORS dependence on optical and spatial properties, respectively.

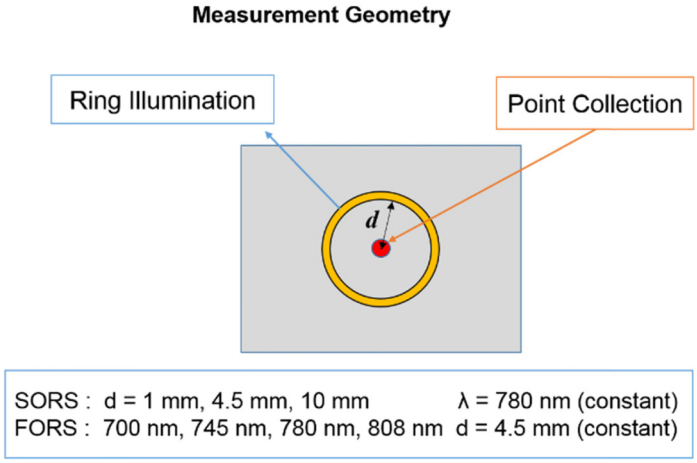

Fig. 3. Pictorial description and key parameters of the measurement geometry.

Raman spectra were collected in the spectral region from 500 to 1600 cm^{-1}, with a spectral resolution of 10 cm^{-1}. Measurements were carried out with power on the sample around 95 mW at all excitation wavelengths, over an acquisition time of 20 s. Following data acquisition, spectral calibration was performed with the aid of two reference samples (trigonal calcite at 713 and 1087 cm^{-1}, gypsum at 415, 495, 1009 and 1141 cm^{-1}). Simple spectral calibration and baseline correction were performed on the Raman spectra presented in the following.

The variation of the relative Raman intensity of bottom and top layers in the recorded spectrum can be evaluated by calculating an enhancement factor, which is defined as follows for SORS (Eq. (1) and FORS (Eq. (2):

$$\eta_{SORS} = \frac{\frac{I(d)_{Bottom}}{I(d)_{Top}}}{\frac{I(d_0)_{Bottom}}{I(d_0)_{Top}}} \quad (1)$$

$$\eta_{FORS} = \frac{\frac{I(\lambda)_{Bottom}}{I(\lambda)_{Top}}}{\frac{I(\lambda_0)_{Bottom}}{I(\lambda_0)_{Top}}} \quad (2)$$

where d_0 and d are the extreme SORS contrast points, which in our case are 1 mm and 10 mm, respectively. Similarly, λ_0 and λ are the two extreme contrast points of FORS measurements and turn out to be 700 and 808 nm, respectively. To estimate the enhancement factor, we calculated intensity average around peak for the desired peaks and used them in the above equations. The enhancement factor evaluates the ratio between the Raman intensity of the bottom layer and of the top layer, normalized to the ratio of the same intensities obtained at the minimum source-detector separation (d = 1mm) in case of SORS measurements (Eq. (1)), and minimum excitation wavelength (λ = 700 nm) in FORS (Eq. (2)). A high enhancement factor represents a high retrievability of the bottom layer spectrum.

4. Results and discussion

Absorption and scattering spectra of the top layer (PDMS) of the two-layer phantom are shown in Fig. 4(a). The vertical lines represent the excitation wavelengths (700 nm, 745 nm, 780 nm, 808 nm) of FORS measurements. The effectiveness of FORS is maximum when the difference between optical properties (μa and μ's) at the excitation wavelengths is maximum. From Fig. 4(a), at 700 nm, the top layer absorption is around 0.18 cm^{-1}, which is 3.75 times higher than the absorption at 808 nm (0.048 cm^{-1}). Similarly, the scattering at 700 nm is around 10 cm^{-1}, which is 1.3 stronger than at 808 nm. These features make it an ideal phantom for FORS measurements. In brief, for the top layer maximum contrast in optical properties is found between 700 and 808 nm, whereas intermediate values can be seen for 745 nm and 780 nm excitation. The optical properties of the bottom layer (marble) are presented in Fig. 4(b). Unlike the top layer, the bottom layer has constant absorption spectrum with μa around 0.035 cm^{-1}. The scattering spectrum shows slope similar to the top layer, but with increased μ's values, ranging between 11 and 15 cm^{-1}.

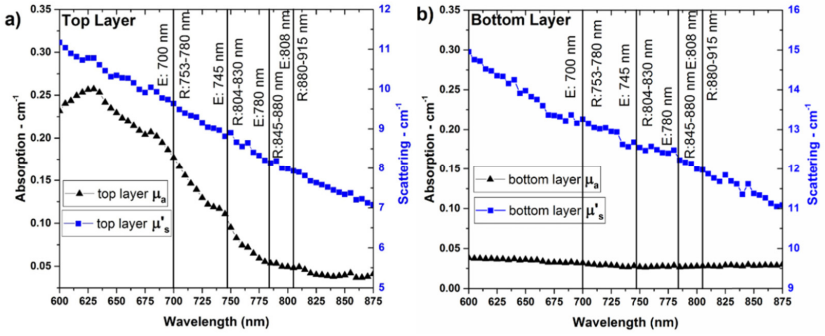

Fig. 4. Absorption (black triangles) and reduced scattering spectrum (blue squares) of the top PDMS layer (a) and of bottom marble layer (b). High contrast is seen in the optical properties of the top layer between 700 and 808 nm. The excitation wavelength E and range R of Raman lines of interest are also reported.

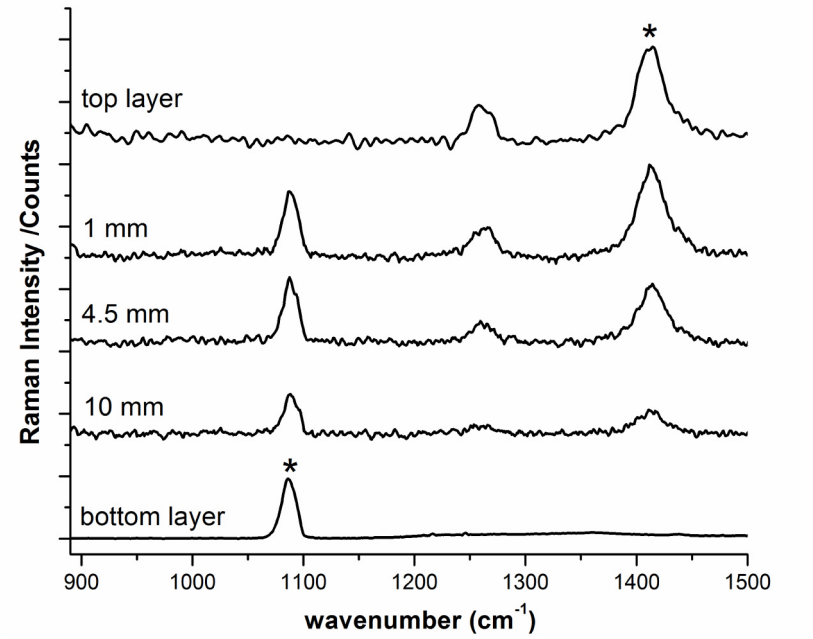

Fig. 5. SORS spectra collected at different source-detector separations (1, 4.5, 10 mm) with excitation source at 780 nm. The asterisk sign denotes the Raman peaks used for evaluating the enhancement factor. All spectra are vertical shifted for clarity.

The results of the first part of the protocol (SORS) are shown in Fig. 5. The pure spectra of the top (PDMS) and bottom (marble) layers are presented at the top and bottom of the plot area, respectively. The spectra at different source-detector separations are vertically shifted and their *d* values are reported next to them for readability. From Fig. 5 it is clear that increasing source-detector separation *d* from 1 to 10 mm increases the Raman signal at 1087 cm^{-1} (*i.e.*, the carbonate peak of calcite, bottom layer), and reduces the contribution from the top layer. The latter can be seen as a reduction in the Raman signal at 1260 and 1411 cm^{-1}, which corresponds to the symmetric and asymmetric stretching of $-CH_3$ vibrations present in PDMS phantom, respectively. An enhancement factor of 2.62 is found between the peak of the top (1087 cm^{-1}) and bottom (1411 cm^{-1}) layers. The obtained results are in-line with SORS measurements performed on biological tissue mimicking phantoms, with optical properties similar to biological tissues [34].

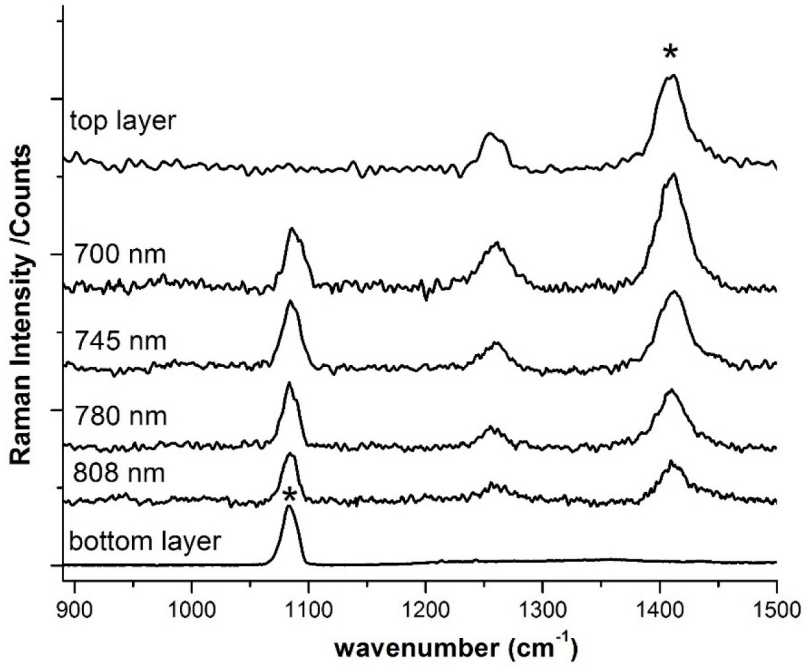

Fig. 6. FORS spectra collected at different excitation source wavelengths (700, 745, 780, 808 nm) with a fixed source-detector separation (d = 4.5 mm). The asterisk sign denotes the Raman peaks used for evaluating the enhancement factor. All spectra are vertical shifted for clarity.

The second part of the study was devoted to FORS. This was performed at four chosen excitation wavelengths (700 nm, 745 nm, 780 nm, 808 nm) on the same 2-layer phantom as SORS, in which the top layer shows a monotonous decrease in optical properties (μ_a and μ'_s) while moving spectrally from 700 to 808 nm. Figure 6 summaries the results of FORS measurements. Similar to what observed with SORS upon changing source-detector separation, here varying contributions to Raman spectra from the top (peak at 1411 cm^{-1}) and bottom (1087 cm^{-1}) layers are seen by changing excitation wavelength. However, unlike SORS, here the changing contribution in spectra is due to changing optical properties rather than spatial distances *d*. Higher absorption and scattering properties at 700 nm prevent the photons from propagating deep into the medium, leading to a strong contribution of the top layer (the peak at 1411 cm^{-1} is higher than the one at 1087 cm^{-1}). As expected, this phenomenon is inverted (peak at 1087 cm^{-1} is higher than at 1411 cm^{-1}) when we moved to 808 nm excitation, where the optical properties of top layer are minimal, letting photons propagate deeper. Though the measurements at all excitations were performed with the same power (95 mW) and despite the higher absorption, a higher Raman signal from the top layer (1411 cm^{-1}) is seen at 700 nm from Fig. 6. This phenomenon can be attributed to the larger values of μ'_s at 700 nm, facilitating stronger Raman scattering interactions, and thus giving rise to higher Raman signal. We ruled out possible effects due to photon collection efficiency, as our system shows comparatively negligible efficiency changes in the measured spectral range. An enhancement factor of 2.81 is observed for FORS measurements, which was calculated by considering the 1411 cm^{-1} peak of the top layer and the 1087 cm^{-1} peak of the bottom layer at 700 nm and 808 nm excitation, respectively.

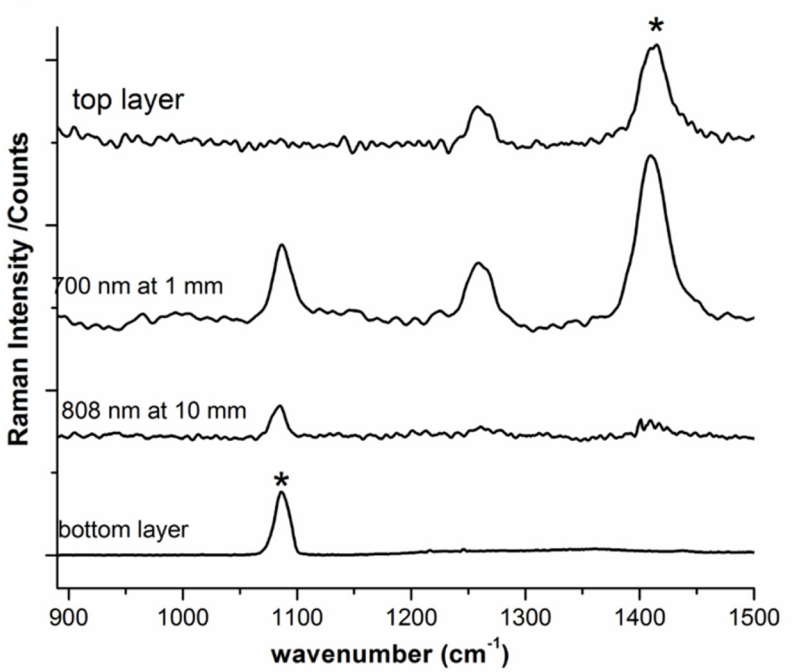

Fig. 7. Hybrid FORS-SORS spectra. The top layer peak at 1411 cm^{-1} almost disappears at 808 nm. The asterisk sign denotes the Raman peaks used for evaluating the enhancement factor. All spectra are vertical shifted for clarity.

It is clear from the above discussion that the SORS and FORS are complementary in nature: to retrieve deep information the former exploits spatial properties, while the other uses optical properties. Interestingly, these two techniques (spatial and optical property dependence) can be combined to get maximum enhancement. This suggested us to propose the hybrid FORS-SORS approach to enhance probing of deep layers in a diffusive medium. As shown pictorially in Fig. 1(c), hybrid FORS-SORS was performed at two extreme conditions. At first, a measurement was performed on the same phantom as previously described at short source-detector separation (d = 1 mm) at 700 nm. This measurement enhanced the signal of the top layer by utilizing both spatial (short d) and optical properties (low μ_a and μ'_s) of the medium, thus effectively employing benefits of both FORS and SORS. The second measurement was performed at 808 nm (d = 10 mm) where the spatial (large d) and the optical properties (high μ_a and μ'_s) are such to enhance the signal from the bottom layer.

From Fig. 7, at 700 nm the peak of the bottom layer (1087 cm^{-1}) is relatively weaker compared to the peak of the top layer (1411 cm^{-1}), whereas the peak of top layer almost disappears in the Raman spectrum acquired at 808 nm with large source-detector separation (d = 10 mm). These extreme contrast measurements at 700 and 808 nm were used for enhancement calculations. For the hybrid FORS-SORS technique an enhancement of 6.0 is estimated, significantly higher than for SORS alone (2.62) or FORS alone (2.81).

To better understand and characterize SORS and FORS, we performed both FORS and SORS measurements at all possible combinations, *i.e.*, SORS at all excitations, and FORS at all source-detector separations. Table 2 presents a summary of the results, reporting the enhancement factor of all FORS and SORS measurements. Enhancement calculations were performed using Raman spectra obtained at d_0 = 1 mm and d = 10 mm for SORS. For FORS, Raman spectra obtained at λ_0 = 700 nm and λ = 808 nm were used. From Table 2, SORS has reduced enhancement with increasing optical properties, showing a minimum of 2.15 at 700

nm, where the absorption and scattering of top layer are maximum. Instead, the advantage of SORS is its increased enhancement (2.80) when the optical properties of medium are minimal. Interestingly, an increase in enhancement (2.99) is seen for FORS at short source-detector separation (d = 1 mm). This is an important advantage of FORS, which can increase the spatial resolution in a tomographic approach to FORS measurements, provided it is confirmed as a general observation, independent of the specific phantom considered here. Moreover, in SORS, SNR is limited due to the large source-detector separation, where the high d value is a key factor for high enhancement, while FORS has significantly higher SNR due to the minimal source-detector separation, which is a key factor for high enhancement.

Table 2. Enhancement factor of FORS and SORS measurements at multiple source-detector separations (d) and excitations. Bold values in the table represent the enhancement factor.

		d = 1 mm	d = 4.5 mm	d = 10 mm
FORS		**2.99**	**2.81**	**2.60**
	700 nm	745 nm	780 nm	808 nm
SORS	**2.15**	**2.39**	**2.62**	**2.80**
	700 nm d = 1 mm		808 nm d = 10 mm	
FORS-SORS		**6.00**		

It is important to discuss also the limitations of FORS. First of all, as stated in Section 2, FORS can be applied only when it is possible to achieve a significant difference in optical properties between a couple of not-too-far excitation wavelengths. For biological media this could happen, for example, in the 600-700 nm region, where a significant decrease of hemoglobin absorption accompanied by a decrease in scattering are observed. In other cases, as for powders, the absorption spectrum could happen to be flat, nonetheless depth contrast could still be achieved for a decreasing scattering spectrum. Surely, the medium optical properties must be known before performing a FORS measurement. A different concern is due to the changes of optical properties for the Raman lines produced by the two different excitation wavelengths, causing uneven depth sensitivity over the whole Raman spectrum. As a consequence, the direct scaled subtraction of the two Raman spectra – as typically implemented for SORS [8] – could be not fully applicable. Still, also for SORS the natural changes of optical properties with Raman frequencies translates into different signal attenuation at different source-detector distances. In both cases, proper modelling of diffuse Raman propagation should be adopted instead of simple subtraction – yet at the cost of higher complexity. A further issue is contamination by fluorescence contributions. While in SORS the single excitation wavelength can be chosen to optimize both depth penetration and fluorescence suppression, conversely in FORS the need of a second lower-wavelength excitation exhibiting significant optical changes can bring along some higher fluorescence contribution. Finally, there are clearly different challenges in the SORS and FORS instrumentation. While in SORS the issue is to have a probe and system setup accepting multi-distance spectral acquisitions, conversely in FORS the problem is on the change in excitation wavelength, forcing to switch among different excitation and collection filter sets.

Measurements were performed on a very simple two-layer phantom with a distinct and intense Raman peak from the bottom layer, which permits to clearly calculate the enhancement factors for an easy and reliable comparison between FORS and SORS. In biological media we would expect a more complex situation, with an overlapping of the Raman spectra of the upper and lower layers. Yet, since Raman emission is a linear process, similar enhancement factors are expected for a similar set of optical properties independent of the Raman emission strengths.

5. Conclusion

We propose Frequency Offset Raman Spectroscopy (FORS) as a non-invasive tool to probe the Raman spectrum of deep layers in diffusive media. The technique was successfully demonstrated on a tissue mimicking phantom: an enhancement of 2.62 and 2.81 were found for SORS and FORS measurements, respectively. A brief comparison between SORS and FORS, revealed the complementary nature of the two techniques, with FORS having advantage over SORS with respect to SNR and spatial resolution, as well as a fixed *d* probe. Conversely, FORS requires to exploit medium-specific changes in optical properties, and a Raman system suitable to provide multiple-wavelength excitation. A hybrid FORS-SORS approach was also proposed and demonstrated by combining advantages of both SORS and FORS techniques. An enhancement of 6.0 was obtained, suggesting the hybrid approach can further enhance the bottom layer probing. The proposed techniques (FORS, hybrid FORS-SORS) may have great importance to biological media, especially in an *in vivo* scenario where the absorption spectral variation of tissue constituents (hemoglobin around 650 nm, lipid and water around 960 nm) can be exploited to extract Raman signal of deep tissues, like human bone, for diagnostic purposes.

Funding

This work was supported by OILTEBIA (Optical Imaging and Laser TEchniques for BIomedical Applications) under Grant No. 317526.

Acknowledgments

This work was supported by OILTEBIA (Optical Imaging and Laser TEchniques for BIomedical Applications) under Grant No. 317526. SKVS is Marie Curie fellow funded by the OILTEBIA Project.